Structural and kinetic characterisation of Trypanosoma congolense pyruvate kinase

Structural and kinetic characterisation of *Trypanosoma congolense* pyruvate kinase

Joar Esteban Pinto Torres[a], Meng Yuan[b,c], Julie Goossens[a], Wim Versées[d,e], Guy Caljon[f], Paul A. Michels[c], Malcolm D. Walkinshaw[c], Stefan Magez[a,g,*], Yann G.-J. Sterckx[h,*]

[a] *Research Unit for Cellular and Molecular Immunology (CMIM), Vrije Universiteit Brussel, Pleinlaan 2, B-1050 Brussels, Belgium*
[b] *Current address: Department of Integrative Structural and Computational Biology, The Scripps Research Institute, La Jolla, CA 92037, USA*
[c] *Centre for Translational and Chemical Biology, School of Biological Sciences, The University of Edinburgh, Michael Swann Building, The King's Buildings, Max Born Crescent, Edinburgh EH9 3BF, United Kingdom*
[d] *VIB-VUB Center for Structural Biology, Pleinlaan 2, 1050 Brussels, Belgium*
[e] *Structural Biology Brussels, Vrije Universiteit Brussel, Pleinlaan 2, B-1050 Brussels, Belgium*
[f] *Laboratory of Microbiology, Parasitology and Hygiene (LMPH) and the Infla-Med Centre of Excellence, University of Antwerp, Campus Drie Eiken, Universiteitsplein 1, 2610 Wilrijk, Belgium*
[g] *Ghent University Global Campus, Songdomunhwa-Ro 119, Yeonsu-Gu, 406-840 Incheon, South Korea*
[h] *Laboratory of Medical Biochemistry (LMB) and the Infla-Med Centre of Excellence, University of Antwerp, Campus Drie Eiken, Universiteitsplein 1, 2610 Wilrijk, Belgium*

Abstract

Trypanosoma are blood-borne parasites and are the causative agents of neglected tropical diseases (NTDs) affecting both humans and animals. These parasites mainly rely on glycolysis for their energy production within the mammalian host, which is why trypanosomal glycolytic enzymes have been pursued as interesting targets for the development of trypanocidal drugs. The structure-function relationships of pyruvate kinases (PYKs) from trypanosomatids (*Trypanosoma* and *Leishmania*) have been well-studied within this context. In this paper, we describe the structural and enzymatic characterization of PYK from *T. congolense* (*Tco*PYK), the main causative agent of Animal African Trypanosomosis (AAT), by employing a combination of enzymatic assays, thermal unfolding studies and

*These authors contributed equally to this work and should be considered joint senior authors

Email address: yann.sterckx@uantwerpen.be (Yann G.-J. Sterckx)

X-ray crystallography.

Keywords: X-ray crystallography, enzyme kinetics, Trypanosomes, glycolysis, pyruvate kinase

---

1. Introduction

Glycolysis represents one of the most conserved metabolic pathways across all kingdoms of life. The last reaction of this 10-step cascade is catalyzed by the enzyme pyruvate kinase (PYK), which transfers the phosphate group from phosphoenolpyruvate (PEP) to an ADP molecule in order to produce ATP and pyruvate. This requires the presence of K^+ and Mg^{2+} as co-factors [1]. Because of their role in ATP production and distribution of fluxes into different metabolic branches, the activity of PYKs is usually tightly regulated. Depending on the organism, this may be achieved through i) the generation of different isoforms [2], ii) post-translational modifications [3, 4, 5, 6], and/or iii) binding of multiple allosteric effector molecules [7, 8, 9, 10, 11]. In the context of the latter mechanism, the effector fructose 1,6-bisphosphate (F16BP) has been identified as the most common allosteric activator of PYKs across different species [7, 8, 12, 13]. However, variations on this theme exist as the activity of some PYKs are modulated only by other effectors [11, 14, 15, 16, 17, 18].

In trypanosomatid parasites, such as *Trypanosoma* and *Leishmania*, a large part of the glycolysis occurs inside specialized peroxisomes called glycosomes [19, 20, 21], which house the first seven glycolytic enzymes involved in the conversion of glucose into 3-phosphoglycerate. The remaining downstream reactions (including the one catalyzed by PYK) are carried out in the parasite's cytosol. Like most PYKs, trypanosomatid PYKs are homotetramers. The PYK monomer is a ∼55 kDa protein organized into four domains termed "N", "A", "B", and "C" (Figure 1A). The A domain (residues 19-89 and 188-358), which constitutes the largest part of the PYK monomer, is characterized by an $(\alpha/\beta)_8$-TIM barrel fold that harbors the active site. Together with the N-terminal domain (residues 1-18), it is also involved in the formation of the AA' dimer interface in the PYK

tetramer. The B domain (residues 90-187) is known as the flexible "lid" domain that shields the active site during enzyme-mediated phosphotransfer. Finally, the C domain (residues 359-499) harbors the binding pocket for allosteric effectors and stabilizes the PYK tetramer by formation of CC' dimer interfaces. Interestingly, unlike for most PYKs, fructose 2,6-bisphosphate (F26BP) is a much more potent allosteric activator of trypanosomatid PYKs compared to F16BP [22, 23, 24].

The allosteric regulation of trypanosomatid PYKs has been extensively studied and can be explained via the so-called "rock-and-lock" model coined by Morgan and co-workers [10]. In the absence of substrates (PEP and ADP) and effectors (F26BP or F16BP), trypanosomatid PYKs reside in an inactive and relatively unstable (and flexible) T-state. The binding of substrates causes the enzyme to "rock". This consists of several structural rearrangements across the entire PYK tetramer that involve i) AC-core rotation of 6°-8° (with residues 430-434 as a pivot point), ii) closing of the lid domain (rotation of 30°-40°), iii) stabilization of the AA' dimer interfaces, and iv) flipping of the Arg311 side chain as part of remodeling the catalytic pocket for substrate accommodation. While the "rocked" substrate-bound form (R-state) of PYK is committed to catalysis, in the absence of effectors, trypanosomatid PYKs are characterized by sigmoidal kinetics and display lower specificity constants ($k_{cat}/S_{0.5}$ values) for their substrate PEP compared to their effector-bound form. The binding of effectors to PYK's C domain generates a "lock" in addition to the "rock". This prompts the enzyme to adopt a conformation primed for efficient catalysis; this involves i) the 6°-8° AC-core rotation ii) stabilization of the CC' dimer interfaces through salt bridge formation, and iii) the Arg311 flip. Under these conditions, PYK resides in a stabilized "rocked and locked" state, which has a significantly higher specificity constant and displays hyperbolic kinetics in relation to the binding of its substrates [25]. Hence, PYK is only fully committed to highly efficient catalysis when both its substrates and effectors are bound. Obtaining a detailed understanding of the structure-function relationship of trypanosomatid glycolytic enzymes is important, because they represent attractive targets for

the development of anti-trypanosomal drugs [26, 27, 28].

In this paper, we present an enzymatic and structural characterization of PYK from *T. congolense* (*Tco*PYK), the main causative agent of Animal African Trypanosomosis (AAT). Through enzymatic assays, we show that, as expected, the enzyme's specificity constant increases upon addition of the allosteric effectors (F16BP or F26BP). However, changes are substantially smaller for *Tco*PYK compared to *T. brucei* PYK (*Tbr*PYK), which is one of the reference models for the behavior of trypanosomatid PYKs [29]. Despite this subtle difference, thermal stability experiments suggest that the *Tco*PYK mechanism of action can still be explained by the "rock-and-lock" model described for other trypanosomatid PYKs. In addition, two R-state crystal structures of *Tco*PYK are discussed: *Tco*PYK in complex with i) its allosteric effector F16BP and ii) citrate, which occupies the enzyme's active site.

2. Materials and Methods

2.1. Cloning, protein production, and purification

All details concerning cloning, protein production, and protein purification of *Tco*PYK have been previously described [30]. *Tbr*PYK was obtained by applying the same protocols.

2.2. Enzyme kinetics

The activity assays and enzyme kinetics of *Tco*PYK were measured and determined in a similar manner as for *Tbr*PYK [29] with some minor modifications. Briefly, the activity of the enzyme was measured by following the decay of NADH absorbance at 340 nm in a lactate-dehydrogenase (LDH)-coupled system, ensuring that the *Tco*PYK-catalyzed reaction is rate limiting. Enzyme activity was measured at 25°C in a 100 μl reaction mixture containing 50 mM triethanolamine (TEA) buffer pH=7.2, 10 mM $MgCl_2$, 100 mM KCl, 0.5 mM NADH (Sigma-Aldrich N8129) and 3.2 U of LDH from rabbit muscle (Sigma-Aldrich L1254-5KU). The substrates (PEP and ADP) and the effectors (F16BP and F26BP) were added as indicated further below. *Tco*PYK was diluted in assay buffer (50 mM TEA buffer pH=7.2, 10 mM $MgCl_2$, 100 mM KCl) to a final concentration of 2.5 μg ml^{-1}.

Enzyme kinetics with regards to PEP were studied at saturating concentrations of ADP (2 mM) and variable concentrations of PEP ranging from 0 mM to 5 mM in the presence or absence of F16BP (2.5 mM) or F26BP (2 μM). After adding all reagents in the reaction mixture, the decrease in absorbance at 340 nm was monitored for 5 minutes using a microplate reader spectrophotometer (SpectraMax Plus 384, Molecular Devices). The data were analyzed using SoftMax Pro7 software (Molecular Devices).

Depending on the type of kinetics obtained, the initial rates of NADH oxidation where determined and fitted using equations 1 or 2. For hyperbolic kinetics, equation 1 was employed

$$V_0 = \frac{V_{max} \cdot [S]}{K_M + [S]} \quad (1)$$

where V_0, V_{max}, $[S]$ and K_M refer to the initial reaction rate, the enzyme's maximum rate, the substrate concentration (mM) and the Michaelis-Menten constant of *Tco*PYK, respectively.

For sigmoidal kinetics, equation 2 was used

$$V_0 = \frac{V_{max} \cdot [S]^{n_H}}{S_{0.5}^{n_H} + [S]^{n_H}} \quad (2)$$

where $S_{0.5}$ and n_H indicate the substrate concentration giving half-maximal reaction rate (mM) and Hill coefficient, respectively. The turnover number (k_{cat}) was calculated by the dividing the maximal velocity by the molar enzyme concentration (using the subunit molar mass of 56348 g mol[1]). The specificity constant of *Tco*PYK was obtained by determining the ratios k_{cat}/K_M or $k_{cat}/S_{0.5}$.

For the citrate inhibition experiments, the set-up described above was employed at 5 mM PEP with the addition of several citrate concentrations ranging from 0 mM to 25 mM.

2.3. Differential scanning fluorimetry

Differential scanning fluorimetry (DSF) experiments were performed to determine the apparent melting temperatures ($T_{m,app}$) of *Tco*PYK in the presence and absence of its effector F16BP and substrate PEP. DSF was performed on a CFX Connect Real-Time System Thermal Cycler (Bio-RAD). Data were collected from 10°C to 95°C at a scan rate of 1°C min^{-1}. The fluorescence signal was recorded every 0.5°C. Experiments were carried out in 96-well plates and the total sample volume was 25 μl. To determine the optimal protein-dye ratio, a grid screen of various concentrations of SYPRO orange dye (Life Technologies) (ranging from 0x to 100x) and *Tco*PYK (ranging from 0 μM to 50 μM) was carried out. After identification of a suitable condition (10x SYPRO orange dye and 5 μM *Tco*PYK), the $T_{m,app}$ of the enzyme was measured in assay buffer

(20 mM Tris-HCl, 150 mM NaCl, 10 mM $MgCl_2$, 100 mM KCl, pH 7.2) in the presence and absence of F16BP (5 mM), PEP (10 mM), and citrate (25 mM and 50 mM). All experiments were conducted in triplicate.

2.4. Crystallization, data collection and processing, and structure determination

*Tco*PYK was concentrated to 4 mg ml^{-1} using a 50,000 molecular weight cut-off concentrator (Sartorius Vivaspin20). Crystallization conditions were screened manually using the hanging-drop vapor-diffusion method in 48-well plates (Hampton VDX greased) with drops consisting of 2 μl protein solution and 2 μl reservoir solution equilibrated against 150 μl reservoir solution. Commercial screens from Hampton Research (Crystal Screen, Crystal Screen 2, Crystal Screen Lite, Index, Crystal Screen Cryo), Molecular Dimensions (MIDAS, JCSG+), and Jena Bioscience (JBScreen Classic 1–10) were used for initial screening. The affinity tag was retained for crystallization. The crystal plates were incubated at 20°C. Diffraction-quality crystals of apo *Tco*PYK were obtained in an optimized variant of the JCSG+ (Molecular Dimensions) condition no. 3 (100 mM ammonium citrate dibasic, 12.5% PEG 3350) and the crystals grew after approximately 14 days. For *Tco*PYK-F16BP, diffraction quality crystals were obtained in an optimized variant of the JBScreen Classic 4 (Jena Bioscience) condition no. D3 (50 mM magnesium acetate, 225 mM sodium acetate, 10% PEG 8000 and 2.5 mM F16BP) and the crystals grew after a couple of weeks.

The apo *Tco*PYK and *Tco*PYK-F16BP crystals were cryocooled in liquid nitrogen with the addition of 30% (v/v) and 25% (v/v) glycerol, respectively, to the mother liquor as a cryoprotectant in 5% increments. Data sets for the apo *Tco*PYK and *Tco*PYK-F16BP crystals were collected on the PROXIMA1 beamline at the SOLEIL synchrotron (Gif-Sur-Yvette, France) and i03 beamline at the DIAMOND synchrotron (Didcot, United Kingdom), respectively. Both data sets were processed with XDS [31]. The quality of the collected data sets was verified by close inspection of the XDS output files and through *phenix.xtriage* in the PHENIX package [32]. Twinning tests were also performed

by *phenix.xtriage*. Analysis of the unit cell contents was performed with the program MATTHEWS-COEF, which is part of the CCP4 package [33]. The structure of apo *Tco*PYK was determined by molecular replacement with PHASER-MR [34]. The structure of the *Tbr*PYK tetramer (PDB ID: 4HYV [29]) was used as a search model. Given its notorious flexibility, the B domain of the enzyme was deleted for the molecular replacement. This provided a single solution (top TFZ = 71.1 and top LLG = 6130.8). The structure of *Tco*PYK-F16BP was determined by using the crystal structure of apo *Tco*PYK as a search model for molecular replacement. Here, a CC' interface dimer devoid of its B domains was employed to search for four copies, which resulted in two quasi identical solutions (top TFZ = 68.7 and top LLG = 4415.6). For both structures, refinement cycles using BUSTER-TNT [35] or the maximum likelihood target function cycles of *phenix.refine* [36] were alternated with manual building using Coot [37]. The final resolution cut-off was determined through the paired refinement strategy [38], which was performed on the PDB-REDO server [39]. The crystallographic data for the apo *Tco*PYK and *Tco*PYK-F16BP structures are summarized in Table 1 and have been deposited in the PDB (PDB IDs: 6SU1 and 6SU2, respectively). Molecular graphics and analyses were performed with UCSF Chimera [40].

Table 1: **Data collection and refinement statistics.** Statistics for the highest resolution shell are shown in parentheses.

	***Tco*PYK-citrate**	***Tco*PYK-F16BP**
Data collection statistics		
Wavelength (Å)	0.97903	0.99989
Resolution range (Å)	49.33 - 3.0 (3.107 - 3.0)	42.74 - 3.0 (3.107 - 3.0)
Space group	aP: P1	oI: I222
a, b, c (Å)	83.45, 107.15, 148.00	112.77, 182.46, 244.85
α, β, γ (°)	109.7, 90.51, 106.78	90.00, 90.00, 90.00
Mosaicity (°)	0.390	0.053
Total number of measured reflections	167758 (17254)	691994 (68236)
Unique reflections	85798 (8940)	50876 (5019)
Multiplicity	2.0 (1.9)	13.6 (13.6)
Completeness (%)	93.36 (97.01)	99.89 (99.90)
$< I/\sigma(I) >$	6.20 (0.91)	12.18 (0.88)
Wilson B-factor (Å^2)	77.63	102.33
R_{meas} (%)	14.69 (114.60)	20.09 (271.80)
$CC_{1/2}$ (%)	0.989 (0.364)	0.998 (0.347)
CC*	0.997 (0.731)	1.000 (0.718)
A.U. contains	2 tetramers	2 dimers
Refinement statistics		
CC_{work}	0.879 (0.536)	0.933 (0.404)
C_{free}	0.824 (0.434)	0.941 (0.284)
R_{work} (%)	24.76 (33.01)	27.32 (44.09)
R_{free} (%)	29.46 (37.16)	30.43 (50.92)
Number of non-hydrogen atoms	28228	14203
macromolecules	27895	14070
ligands	155	84
solvent	178	49
Protein residues	3765	1974
RMS bond lengths (Å)	0.014	0.013
RMS bond angles (°)	1.91	1.85
Ramachandran favored (%)	92.23	94.04
Ramachandran allowed (%)	7.21	5.40
Ramachandran outliers (%)	0.56	0.56
Rotamer outliers (%)	3.13	3.65
Clashscore	12.83	14.37
Overall MolProbity score	2.47	2.49
Average B-factor (Å^2)	86.62	104.79
macromolecules	86.77	104.64
ligands	102.04	150.39
solvent	50.03	71.44
PDB ID	6SU1	6SU2

3. Results and Discussion

3.1. The allosteric effectors F16BP and F26BP increase the specificity constant of Tco*PYK towards PEP*

The PYK family is well-conserved within the group of kinetoplastids (at least 60% sequence identity), and even more so among members of the *Trypanosoma* genus (at least 80% sequence identity). *Tco*PYK shares high sequence identity with *Tbr*PYK (88.0%; Figure 1B), which has been extensively studied in terms of structure and enzymatic mechanism [23, 29]. *Tco*PYK displays an enzymatic behavior similar to *Tbr*PYK, as was expected given the high degree of sequence conservation within the trypanosomatid PYK family. The kinetics of both enzymes in the absence of the allosteric effectors F16BP or F26BP can be described by a sigmoidal curve (Hill coefficient $n_H > 1$) of which the parameters are reported in Table 2. In addition, both enzymes display typical features of trypanosomatid PYKs [10, 25, 29]: i) the effectors F16BP and F26BP increase the specificity constants ($k_{cat}/S_{0.5}$ values), mainly due to a decreased $S_{0.5}$ value, and ii) F26BP is a more potent allosteric regulator since its effects are exerted at micromolar concentrations (compared to millimolar concentrations for F16BP). A noteworthy observation is the significantly smaller rise in specificity constant for *Tco*PYK (factor of ∼2) compared to *Tbr*PYK (factor of ∼6). This may suggest that the allosteric effectors F16BP and F26BP have a lower impact on the specificity constant of *Tco*PYK towards PEP in comparison with *Tbr*PYK.

3.2. Thermal unfolding studies demonstrate that effector and substrate binding increase Tco*PYK's thermal stability*

One of the main features of the "rock-and-lock" model is the difference in thermal stability of the various PYK states due to the rigidification of specific regions within the tetramer. Thermal unfolding studies for *L. mexicana* PYK (*Lme*PYK), *T. cruzi* (*Tcr*PYK) and *Tbr*PYK have shown the following general trend in terms of protein stability: apo (T-state) < substrate-bound (R-state) < effector-bound (R-state) < substrate and effector-bound (R-state) [10, 25, 29].

Figure 1: **Structure-sequence relationship for trypanosomatid PYKs.** (A.) The left panel displays the PYK monomer. The different domains are color-coded, and the domain boundaries are shown. The pivot point for the AC core rotation (residues 430-433 for *Tco*PYK) is indicated by a magenta arrow. The right panel shows the PYK tetramer and the AA' and CC' dimer interfaces are indicated by dashed lines. The substrate and effectors binding sites are highlighted by yellow and cyan boxes, respectively. (B.) Sequence alignment of *Tco*PYK (Uniprot ID G0UYF4) and *Tbr*PYK (Uniprot ID P30615). The green bar above the sequence alignment represents all identical amino acids, whereas those indicated by a black bar are different. The residues marked by the colored circles are involved in interface interactions, substrate and metal binding, and effector binding (see boxed legend for more details). The pivot point and effector loop amino acids are indicated by magenta and cyan boxes, respectively. Arg311 is highlighted by a yellow box.

Table 2: **Comparison of kinetic properties of recombinant *Tco*PYK and *Tbr*PYK.**

Substrate	**Effector**	**Kinetic parameters**	***Tco*PYK**	***Tbr*PYK**[1]	***Tbr*PYK**[2]
PEP	None	$S_{0.5}$ (mM)	0.65 ± 0.18	1.88 ± 0.04	1.03 ± 0.08
		n_H	1.70 ± 0.09	2.28 ± 0.02	1.88 ± 0.12
		k_{cat} (min^{-1})	5.21 ± 1.26 ($\times 10^3$)	6.26 ± 0.65 ($\times 10^3$)	8.72 ± 0.16 ($\times 10^3$)
		$k_{cat}/S_{0.5}$ (mM^{-1} min^{-1})	8.79 ($\times 10^3$)	3.33 ($\times 10^3$)	8.49 ($\times 10^3$)
PEP	F26BP	$S_{0.5}$ (mM)	0.38 ± 0.12	0.49 ± 0.10	0.12 ± 0.02
		n_H	1.00 ± 0.07	1.56 ± 0.02	1.19 ± 0.10
		k_{cat} (min^{-1})	6.69 ± 0.03 ($\times 10^3$)	9.12 ± 1.46 ($\times 10^3$)	13.86 ± 0.26 ($\times 10^3$)
		$k_{cat}/S_{0.5}$ (mM^{-1} min^{-1})	18.36 ($\times 10^3$)	20.03 ($\times 10^3$)	117.00 ($\times 10^3$)
PEP	F16BP	$S_{0.5}$ (mM)	0.33 ± 0.04	0.39 ± 0.01	0.26 ± 0.04
		n_H	2.32 ± 0.29	1.99 ± 0.05	1.31 ± 0.09
		k_{cat} (min^{-1})	6.44 ± 0.88 ($\times 10^3$)	7.07 ± 1.46 ($\times 10^3$)	11.10 ± 0.23 ($\times 10^3$)
		$k_{cat}/S_{0.5}$ (mM^{-1} min^{-1})	19.03 ($\times 10^3$)	19.58 ($\times 10^3$)	42.70 ($\times 10^3$)

[1]This work (recombinantly produced, His-tagged protein)

[2][29] (recombinantly produced, untagged protein)

Figure 2: **Differential scanning fluorimetry measurements.** The thermal stability profiles of *Tco*PYK in the absence and presence of substrates and/or effectors. The experimental data are plotted under a differentiated form in which the curve peaks correspond to the $T_{m,app}$ values.

Differential scanning fluorimetry (DSF) experiments conducted on *Tco*PYK in the presence and absence of PEP and/or F16BP demonstrate that the enzyme displays a thermal stability profile typical of trypanosomatid PYKs (Figure 2). While unligated *Tco*PYK has an apparent melting temperature ($T_{m,app}$) of ∼46.0°C, the enzyme is clearly stabilized by the addition of its substrate PEP ($\Delta T_{m,app} \approx 12.0$°C), its effector F16BP ($\Delta T_{m,app} \approx 11.5$°C), or both PEP and F16BP ($\Delta T_{m,app} \approx 17.0$°C; Figure 2). As has been described for other trypanosomatid PYKs [10, 25, 29], the increasing thermal stability of the enzyme upon binding of substrates and/or effectors most likely reflects a decrease in conformational flexibility and, thus, rigidification of the *Tco*PYK tetramer. When compared to the enzyme kinetics (Table 2), it is clear that the enhancement in *Tco*PYK's specificity constant towards PEP correlates with an increased thermal stability. These are characteristic features of the mechanistic principles underlying trypanosomatid PYK function according to the "rock-and-lock" model [10].

3.3. Tco*PYK adopts an R-state conformation when bound by its effector F16BP*

Given that F16BP also allosterically regulates the function of trypanosomatid PYKs, F16BP is expected to prompt similar structural rearrangements in the PYK tetramer as observed for F26BP [29]. However, a structure of a trypanosomatid PYK in complex with F16BP has not yet been reported. Therefore, *Tco*PYK was crystallized in complex with its effector F16BP. The crystal structure of *Tco*PYK bound with F16BP displays a characteristic R-state conformation also observed for the *Tbr*PYK-F26BP complex (Figure 3): i) rotation of the AC core by 6°-8° around residues 430-434 as a pivot point, ii) the formation of a hydrogen bond between A domain Arg311 and the backbone carbonyl groups of Arg263 and Gly264 in the adjacent A' domain (and *vice*

versa) in order to remodel the catalytic pocket for substrate accommodation, and iii) binding of F16BP or F26BP by the effector pocket to fix the otherwise flexible effector binding loop and stabilize the CC' dimer interface. Hence, as has been described for F26BP, F16BP binding provides a "lock", which involves rigidification of certain regions of the *Tco*PYK tetramer (fixation of the effector binding loop and CC' dimer interface stabilization due to salt bridge formation). Taken together with the kinetic and thermal unfolding data discussed above, this loss of flexibility correlates with an improved thermal stability and, importantly, with an enhancement of enzyme activity (*i.e.* increase in specificity constant) as has been described for F26BP [29].

The structural changes in effector loop conformation upon effector binding have been well-documented for F16BP [41] and F26BP [25] binding to human and trypanosomatid PYKs, respectively. As discussed by Morgan and colleagues [25], the effector loop conformations and orientations of the bound effector are markedly different for F16BP-human PYK compared to F26BP-trypanosomatid PYK complexes. In the *Tco*PYK-F16BP structure presented here, the observed effector loop conformation and effector molecule orientation are both highly similar to those reported for the *Tbr*PYK-F26BP complex (Figure 3). While the residues mediating the protein-effector interactions are identical, certain differences exist in the way the effectors are accommodated into the effector binding pocket (Table 3). While the interactions mediating accommodation of the effector's C6 phosphate group are virtually identical in both cases, main differences exist in the binding of the other substituents of the effector molecule. Noteworthy differences compared to the *Tbr*PYK-F26BP structure are: i) the apparently weaker hydrogen bond between *Tco*PYK Asn402 and the F16BP C1 phopshate, ii) the seemingly weaker salt bridge between *Tco*PYK Arg454 and the F16BP C1 phopshate, iii) the different orientation of Arg457 in the accommodation of the F16BP C1 phosphate ("lateral" salt bridge between Arg457 side chain NH2 compared to a "frontal" salt bridge between *Tbr*PYK Arg457 and the F26BP C2 phosphate involving both the Arg457 side chain NH1 and NH2 groups), and iv) the lack of an interaction between

Figure 3: **Structural features of F16BP-bound *Tco*PYK.** For both (A.) and (B.), the left panel displays a superposition of apo *Tcr*PYK (PDB ID 4KRZ [25]) and *Tco*PYK-F16BP (PDB ID 6SU2, this work), which illustrates the AC core rotation. Apo *Tcr*PYK is colored sky blue, while the *Tco*PYK-F16BP is color-coded according to Figure 1A. In each monomer, the locations of Arg311 and the effector binding site are highlighted by yellow and cyan boxes, respectively. The right panels in both (A.) and (B.) depict stereo views of the regions highlighted by the boxes. (A.) Overview of the interactions made by Arg311 within the PYK AA' interface. The top stereo view highlights this region for apo *Tcr*PYK (colored in sky blue), while the bottom stereo view presents a superposition of *Tco*PYK-F16BP (colored as in Figure 1A) and *Tbr*PYK-F26BP (colored in light grey; PDB ID 4HYW [29]). Residues Arg263, Gly264, Gln298, Arg311 and Asp316 are shown in stick representation. The residues originating from the A' domain are indicated by an asterisk '*'. (B.) Overview of the interactions made within the effector binding site comprising the effector binding loop (Ala482-Gly488). The top stereo view highlights this region for apo *Tcr*PYK (colored in sky blue), while the bottom stereo view presents a superposition of *Tco*PYK-F16BP (colored as in Figure 1A) and *Tbr*PYK-F26BP (colored in light grey; PDB ID 4HYW [29]). Residues Leu400, Ser401, Asn402, Ser/Thr403, Ser406, Arg/Lys454, Arg457, Tyr489 and Pro490 are shown in stick representation.

the Gly488 backbone amide and the C1 OH, which is obviously not present in F16BP (instead, the Gly488 backbone amide only forms a hydrogen bond with the hemiketal oxygen of F16BP). Overall, given reduced number of interactions between F16BP and *Tco*PYK and the longer distances (and thus presumably weaker interactions) within the *Tco*PYK-F16BP complex, these data might explain why F26BP is a more potent activator of trypanosomatid PYKs compared to F16BP. However, given the moderate resolution of the structure and sometimes weak electron density in this region of the crystal, additional validation will require collecting higher resolution data sets. Despite our efforts, we have not succeeded in acquiring such data sets yet.

3.4. Citrate binds Tco*PYK's active site, induces an R-state transition, and is a weak inhibitor of enzyme activity*

Given the availability of an R-state structure for *Tco*PYK, we attempted to obtain a crystal structure of the enzyme in its unligated T-state. Crystallization

Table 3: **Comparison of protein-effector interactions in the *Tbr*PYK-F26BP and *Tco*PYK-F16BP complexes.** *Tbr*PYK-F26BP (PDB ID 4HYW [29]) and *Tco*PYK-F16BP (PDB ID 6SU2, this work). The average distances of interactions are reported and were calculated by measuring all distances within all chains of the respective asymmetric units.

***Tbr*PYK-F26BP**			***Tco*PYK-F16BP**		
*Tbr*PYK	F26BP	Interaction (distance)	*Tco*PYK	F16BP	Interaction (distance)
Leu400 backbone CO	C4 OH	hydrogen bond (2.7 Å)	Leu400 backbone CO	C3 OH	hydrogen bond (3.5 Å)
Ser401 side chain OH	C6 P	hydrogen bond (2.5 Å)	Ser401 side chain OH	C6 P	hydrogen bond (3.6 Å)
Asn402 backbone NH	C6 P	hydrogen bond (2.6 Å)	Asn402 backbone NH	C6 P	hydrogen bond (2.8 Å)
Asn402 side chain NH_2	C2 P	hydrogen bond (3.0 Å)	Asn402 side chain NH_2	C1 P	hydrogen bond (3.7 Å)
Thr403 backbone NH	C6 P	hydrogen bond (2.8 Å)	Thr403 backbone NH	C6 P	hydrogen bond (2.8 Å)
Thr403 side chain OH	C6 P	hydrogen bond (2.9 Å)	Thr403 side chain OH	C6 P	hydrogen bond (3.1 Å)
Ser406 backbone NH	C6 P	hydrogen bond (2.9 Å)	Ser406 backbone NH	C6 P	hydrogen bond (3.2 Å)
Ser406 side chain OH	C6 P	hydrogen bond (2.7 Å)	Ser406 backbone NH	C6 P	hydrogen bond (2.8 Å)
Lys454 side chain N_ζ	C2 P	electrostatic (2.8 Å)	Arg454 side chain NH1	C1 P	electrostatic (3.8 Å)
Arg457 side chain NH1	C2 P	electrostatic (2.7 Å)	/	/	/
Arg457 side chain NH2	C2 P	electrostatic (3.0 Å)	Arg457 side chain NH2	C1 P	electrostatic (2.5 Å)
Ala482 backbone NH	C3 OH	hydrogen bond (3.1 Å)	Ala482 backbone NH	C3 OH	hydrogen bond (3.8 Å)
Gly488 backbone NH	C1 OH	hydrogen bond (2.7 Å)	/	/	/
Gly488 backbone NH	hemiketal O	hydrogen bond (4.0 Å)	Gly488 backbone NH	hemiketal O	hydrogen bond (4.2 Å)
Tyr489 backbone NH	hemiketal O	hydrogen bond (3.4 Å)	Tyr489 backbone NH	hemiketal O	hydrogen bond (4.7 Å)

conditions for apo *Tco*PYK were screened on a large scale by employing various commercial screens. Crystals were finally obtained in an optimized variant of the JCSG+ (Molecular Dimensions) condition no. 3 (100 mM ammonium citrate dibasic, 12.5% PEG 3350). However, structure determination clearly indicated that *Tco*PYK crystallized under these experimental conditions was not unligated and adopted an R-state rather than a T-state conformation. Careful inspection of the electron density revealed that citrate (present in the crystallization cocktail) is bound to *Tco*PYK's active site. The binding of citrate to the active site of PYKs has been documented in two cases: *Homo sapiens* liver PYK (*Hsa*LPYK; PDB ID 4IP7 [42]) and *Cryptosporidium parvum* PYK (*Cpa*PYK; PDB ID 3MA8; paper "to be published"). In both structures, citrate binds at the position where PEP or pyruvate and the γ-phosphate of ATP would normally be located (Figure 4, two top panels). The asymmetric unit of the crystal structure of *Tco*PYK bound by citrate contains 2 tetramers (8 chains). In one chain (chain B), citrate positions itself at a similar location (Figure 4, second panel from the bottom). However, in another chain (chain C), the citrate seems to mimic the triphosphate moiety of ATP (Figure 4, bottom panel). The citrates modeled in all other *Tco*PYK chains adopt poses in between these two extremes. The observed citrate binding site suggests that this metabolite would be able to induce the R-state conformation upon *Tco*PYK binding. Indeed, DSF experiments performed in the absence and presence of citrate clearly support this hypothesis as the addition of citrate increases the protein's thermal stability in a concentration-dependent manner (Figure 5A). The addition of 50 mM citrate causes a similar shift in the protein's apparent melting temperature as observed for 10 mM PEP ($\Delta T_{m,app} \approx 12.0$°C). Since the above-mentioned crystallisation cocktail contained 100 mM ammonium citrate (and no substrates or effectors), this explains the crystallization of *Tco*PYK in its R-state under these conditions.

The presence of citrate in *Tco*PYK's active site could also imply that citrate potentially inhibits its activity through locking the enzyme in a non-productive R-state. Indeed, citrate has been reported to inhibit PYKs from various organ-

Figure 4: **Structural analysis of citrate binding to *Tco*PYK's active site.** Stereo views of superpositions of *Tbr*PYK-PEP-F26BP (PDB ID 4HYV [29]; top panel) with *Lme*PYK-ATP-OXL-F26BP (PDB ID 3HQP [10]), *Hsa*LPYK-CIT (PDB ID 4IP7 [42]; second panel from the top), *Tco*PYK-CIT chain B (PDB ID 6SU1, this work; second panel from the bottom) and *Tco*PYK-CIT chain C (PDB ID 6SU1, this work; bottom panel). The *Tbr*PYK, *Hsa*LPYK and *Lme*PYK structures are colored in light grey, pink and green respectively. The *Tco*PYK structures are color-coded as in Figure 1A. The Mg^{2+} and K^{+} ions are displayed as green and purple spheres, respectively. PEP = phosphoenolpyruvate, OXL = oxalate, CIT = citrate.

Figure 5: **Investigation of the effect of citrate on *Tco*PYK's thermal stability and enzymatic activity.** (A.) The thermal stability profiles of *Tco*PYK in the absence and presence of citrate. The experimental data are plotted under a differentiated form in which the curve peaks correspond to the $T_{m,app}$ values. (B.) The effect of various citrate concentrations on the specific activity of *Tco*PYK at 5 mM PEP.

isms; *Plasmodium falciparum* [43], cyanobacterium *Synechococcus* [44], *Solanum tuberosum* (potato) [45], *Glycine max* (soybean) [46], yeast *Rhodosporidium toruloides* [47], *Hsa*LPYK [42] and *Leishmania major* PYK [48]. In the latter case, the addition of 10 mM citrate leads to a reduction of 50% in enzyme activity. For *Tco*PYK, however, the addition of citrate seems to have very little influence on enzymatic activity: most tested citrate concentrations have no impact whatsoever and weak inhibitory effects are only noticeable starting from 12.5 mM citrate (Figure 5B). Whether or not this citrate-mediated inhibition of *Tco*PYK is physiologically relevant remains unclear and would require further investigation.

In conclusion, the data in this paper demonstrate that *Tco*PYK operates via the "rock-and-lock" model. Although the allosteric effectors F16BP and F26BP appear to have a lesser effect on the specificity constant of *Tco*PYK towards PEP compared with *Tbr*PYK, there seems to be no structural basis to explain this observed discrepancy.

Acknowledgements

This work was supported by the Fonds voor Wetenschappelijk Onderzoek (W.V.), the Hercules foundation (W.V.), a Strategic Research Program Financing of the VUB (W.V., S.M.). The authors wish to thank the staff of the SOLEIL and DIAMOND synchrotrons for outstanding beam line support and dr. Didier Vertommen (UCL, de Duve institute, Belgium) for highly valuable discussions.

References

[1] L. A. Fothergill-Gilmore, P. A. Michels, Evolution of glycolysis, Prog Biophys Mol Biol 59 (2) (1993) 105–235.

[2] E. R. Hall, G. L. Cottam, Isozymes of pyruvate kinase in vertebrates: their physical, chemical, kinetic and immunological properties, Int J Biochem 9 (11) (1978) 785–93.

[3] L. Engström, The regulation of liver pyruvate kinase by phosphorylation–dephosphorylation, Curr Top Cell Regul 13 (1978) 28–51.

[4] M. R. El-Maghrabi, W. S. Haston, D. A. Flockhart, T. H. Claus, S. J. Pilkis, Studies on the phosphorylation and dephosphorylation of L-type pyruvate kinase by the catalytic subunit of cyclic AMP-dependent protein kinase, J Biol Chem 255 (2) (1980) 668–75.

[5] F. Liu, F. Ma, Y. Wang, L. Hao, H. Zeng, C. Jia, Y. Wang, P. Liu, I. M. Ong, B. Li, G. Chen, J. Jiang, S. Gong, L. Li, W. Xu, PKM2 methylation by CARM1 activates aerobic glycolysis to promote tumorigenesis, Nat Cell Biol 19 (11) (2017) 1358–1370. doi:10.1038/ncb3630.

[6] Y. Wei, D. Wang, F. Jin, Z. Bian, L. Li, H. Liang, M. Li, L. Shi, C. Pan, D. Zhu, X. Chen, G. Hu, Y. Liu, C.-Y. Zhang, K. Zen, Pyruvate kinase type M2 promotes tumour cell exosome release via phospho-

rylating synaptosome-associated protein 23, Nat Commun 8 (2017) 14041. doi:10.1038/ncomms14041.

[7] K. Ashizawa, M. C. Willingham, C. M. Liang, S. Y. Cheng, In vivo regulation of monomer-tetramer conversion of pyruvate kinase subtype M2 by glucose is mediated via fructose 1,6-bisphosphate, J Biol Chem 266 (25) (1991) 16842–6.

[8] M. S. Jurica, A. Mesecar, P. J. Heath, W. Shi, T. Nowak, B. L. Stoddard, The allosteric regulation of pyruvate kinase by fructose-1,6-bisphosphate, Structure 6 (2) (1998) 195–210.

[9] A. W. Fenton, M. Hutchinson, The pH dependence of the allosteric response of human liver pyruvate kinase to fructose-1,6-bisphosphate, ATP, and alanine, Arch Biochem Biophys 484 (1) (2009) 16–23. doi:10.1016/j.abb.2009.01.011.

[10] H. P. Morgan, I. W. McNae, M. W. Nowicki, V. Hannaert, P. A. M. Michels, L. A. Fothergill-Gilmore, M. D. Walkinshaw, Allosteric mechanism of pyruvate kinase from *Leishmania mexicana* uses a rock and lock model, J Biol Chem 285 (17) (2010) 12892–8. doi:10.1074/jbc.M109.079905.

[11] W. Zhong, L. Cui, B. C. Goh, Q. Cai, P. Ho, Y. H. Chionh, M. Yuan, A. E. Sahili, L. A. Fothergill-Gilmore, M. D. Walkinshaw, J. Lescar, P. C. Dedon, Allosteric pyruvate kinase-based "logic gate" synergistically senses energy and sugar levels in *Mycobacterium tuberculosis*, Nat Commun 8 (1) (2017) 1986. doi:10.1038/s41467-017-02086-y.

[12] E. B. Waygood, B. D. Sanwal, The control of pyruvate kinases of *Escherichia coli*. I. Physicochemical and regulatory properties of the enzyme activated by fructose 1,6-diphosphate, J Biol Chem 249 (1) (1974) 265–74.

[13] J. D. Dombrauckas, B. D. Santarsiero, A. D. Mesecar, Structural basis for tumor pyruvate kinase M2 allosteric regulation and catalysis, Biochemistry 44 (27) (2005) 9417–29. doi:10.1021/bi0474923.

[14] T. Yamada, J. Carlsson, Glucose-6-phosphate-dependent pyruvate kinase in *Streptococcus mutans*, J Bacteriol 124 (1) (1975) 562–3.

[15] C. Garcia-Olalla, A. Garrido-Pertierra, Purification and kinetic properties of pyruvate kinase isoenzymes of *Salmonella typhimurium*, Biochem J 241 (2) (1987) 573–81. doi:10.1042/bj2410573.

[16] R. Zoraghi, R. H. See, H. Gong, T. Lian, R. Swayze, B. B. Finlay, R. C. Brunham, W. R. McMaster, N. E. Reiner, Functional analysis, overexpression, and kinetic characterization of pyruvate kinase from methicillin-resistant *Staphylococcus aureus*, Biochemistry 49 (35) (2010) 7733–47. doi:10.1021/bi100780t.

[17] H. P. Morgan, F. J. O'Reilly, M. A. Wear, J. R. O'Neill, L. A. Fothergill-Gilmore, T. Hupp, M. D. Walkinshaw, M2 pyruvate kinase provides a mechanism for nutrient sensing and regulation of cell proliferation, Proc Natl Acad Sci U S A 110 (15) (2013) 5881–6. doi:10.1073/pnas.1217157110.

[18] K. Abbe, T. Yamada, Purification and properties of pyruvate kinase from *Streptococcus mutans*, J Bacteriol 149 (1) (1982) 299–305.

[19] F. R. Opperdoes, P. Borst, Localization of nine glycolytic enzymes in a microbody-like organelle in *Trypanosoma brucei*: the glycosome, FEBS Lett 80 (2) (1977) 360–4. doi:10.1016/0014-5793(77)80476-6.

[20] J. R. Haanstra, B. M. Bakker, P. A. M. Michels, In or out? On the tightness of glycosomal compartmentalization of metabolites and enzymes in *Trypanosoma brucei*, Mol Biochem Parasitol 198 (1) (2014) 18–28. doi:10.1016/j.molbiopara.2014.11.004.

[21] B. Szöör, J. R. Haanstra, M. Gualdrón-López, P. A. M. Michels, Evolution, dynamics and specialized functions of glycosomes in metabolism and development of trypanosomatids, Curr Opin Microbiol 22 (2014) 79–87. doi:10.1016/j.mib.2014.09.006.

[22] E. van Schaftingen, F. R. Opperdoes, H. G. Hers, Stimulation of *Trypanosoma brucei* pyruvate kinase by fructose 2,6-bisphosphate, Eur J Biochem 153 (2) (1985) 403–6.

[23] M. Callens, F. R. Opperdoes, Some kinetic properties of pyruvate kinase from *Trypanosoma brucei*, Mol Biochem Parasitol 50 (2) (1992) 235–43. doi:10.1016/0166-6851(92)90220-e.

[24] I. Ernest, M. Callens, F. R. Opperdoes, P. A. Michels, Pyruvate kinase of *Leishmania mexicana mexicana*. Cloning and analysis of the gene, overexpression in *Escherichia coli* and characterization of the enzyme, Mol Biochem Parasitol 64 (1) (1994) 43–54. doi:10.1016/0166-6851(94)90133-3.

[25] H. P. Morgan, W. Zhong, I. W. McNae, P. A. M. Michels, L. A. Fothergill-Gilmore, M. D. Walkinshaw, Structures of pyruvate kinases display evolutionarily divergent allosteric strategies, R Soc Open Sci 1 (1) (2014) 140120. doi:10.1098/rsos.140120.

[26] C. L. Verlinde, V. Hannaert, C. Blonski, M. Willson, J. J. Périé, L. A. Fothergill-Gilmore, F. R. Opperdoes, M. H. Gelb, W. G. Hol, P. A. Michels, Glycolysis as a target for the design of new anti-trypanosome drugs, Drug Resist Updat 4 (1) (2001) 50–65. doi:10.1054/drup.2000.0177.

[27] M.-A. Albert, J. R. Haanstra, V. Hannaert, J. Van Roy, F. R. Opperdoes, B. M. Bakker, P. A. M. Michels, Experimental and in silico analyses of glycolytic flux control in bloodstream form *Trypanosoma brucei*, J Biol Chem 280 (31) (2005) 28306–15. doi:10.1074/jbc.M502403200.

[28] H. P. Morgan, I. W. McNae, M. W. Nowicki, W. Zhong, P. A. M. Michels, D. S. Auld, L. A. Fothergill-Gilmore, M. D. Walkinshaw, The trypanocidal drug suramin and other trypan blue mimetics are inhibitors of pyruvate kinases and bind to the adenosine site, J Biol Chem 286 (36) (2011) 31232–40. doi:10.1074/jbc.M110.212613.

[29] W. Zhong, H. P. Morgan, I. W. McNae, P. A. M. Michels, L. A. Fothergill-Gilmore, M. D. Walkinshaw, 'In crystallo' substrate binding triggers major domain movements and reveals magnesium as a co-activator of *Trypanosoma brucei* pyruvate kinase, Acta Crystallogr D Biol Crystallogr 69 (Pt 9) (2013) 1768–79. doi:10.1107/S0907444913013875.

[30] J. E. Pinto Torres, J. Goossens, J. Ding, Z. Li, S. Lu, D. Vertommen, P. Naniima, R. Chen, S. Muyldermans, Y. G.-J. Sterckx, S. Magez, Development of a Nanobody-based lateral flow assay to detect active *Trypanosoma congolense* infections, Sci Rep 8 (1) (2018) 9019. doi:10.1038/s41598-018-26732-7.

[31] W. Kabsch, XDS, Acta Crystallogr D Biol Crystallogr 66 (Pt 2) (2010) 125–32. doi:10.1107/S0907444909047337.

[32] P. D. Adams, P. V. Afonine, G. Bunkóczi, V. B. Chen, I. W. Davis, N. Echols, J. J. Headd, L.-W. Hung, G. J. Kapral, R. W. Grosse-Kunstleve, A. J. McCoy, N. W. Moriarty, R. Oeffner, R. J. Read, D. C. Richardson, J. S. Richardson, T. C. Terwilliger, P. H. Zwart, PHENIX: a comprehensive Python-based system for macromolecular structure solution, Acta Crystallogr D Biol Crystallogr 66 (Pt 2) (2010) 213–21. doi:10.1107/S0907444909052925.

[33] M. D. Winn, C. C. Ballard, K. D. Cowtan, E. J. Dodson, P. Emsley, P. R. Evans, R. M. Keegan, E. B. Krissinel, A. G. W. Leslie, A. McCoy, S. J. McNicholas, G. N. Murshudov, N. S. Pannu, E. A. Potterton, H. R. Powell, R. J. Read, A. Vagin, K. S. Wilson, Overview of the CCP4 suite and current developments, Acta Crystallogr D Biol Crystallogr 67 (Pt 4) (2011) 235–42. doi:10.1107/S0907444910045749.

[34] A. J. McCoy, R. W. Grosse-Kunstleve, P. D. Adams, M. D. Winn, L. C. Storoni, R. J. Read, Phaser crystallographic software, J Appl Crystallogr 40 (Pt 4) (2007) 658–674. doi:10.1107/S0021889807021206.

[35] O. S. Smart, T. O. Womack, C. Flensburg, P. Keller, W. Paciorek, A. Sharff, C. Vonrhein, G. Bricogne, Exploiting structure similarity in refinement: automated NCS and target-structure restraints in BUSTER, Acta Crystallogr D Biol Crystallogr 68 (Pt 4) (2012) 368–80. doi:10.1107/S0907444911056058.

[36] P. V. Afonine, R. W. Grosse-Kunstleve, N. Echols, J. J. Headd, N. W. Moriarty, M. Mustyakimov, T. C. Terwilliger, A. Urzhumtsev, P. H. Zwart, P. D. Adams, Towards automated crystallographic structure refinement with phenix.refine, Acta Crystallogr D Biol Crystallogr 68 (Pt 4) (2012) 352–67. doi:10.1107/S0907444912001308.

[37] P. Emsley, K. Cowtan, Coot: model-building tools for molecular graphics, Acta Crystallogr D Biol Crystallogr 60 (Pt 12 Pt 1) (2004) 2126–32. doi:10.1107/S0907444904019158.

[38] P. A. Karplus, K. Diederichs, Linking crystallographic model and data quality, Science 336 (6084) (2012) 1030–3. doi:10.1126/science.1218231.

[39] R. P. Joosten, F. Long, G. N. Murshudov, A. Perrakis, The PDB_REDO server for macromolecular structure model optimization, IUCrJ 1 (Pt 4) (2014) 213–20. doi:10.1107/S2052252514009324.

[40] E. F. Pettersen, T. D. Goddard, C. C. Huang, G. S. Couch, D. M. Greenblatt, E. C. Meng, T. E. Ferrin, UCSF Chimera–a visualization system for exploratory research and analysis, J Comput Chem 25 (13) (2004) 1605–12. doi:10.1002/jcc.20084.

[41] J. S. McFarlane, T. A. Ronnebaum, K. M. Meneely, A. Chilton, A. W. Fenton, A. L. Lamb, Changes in the allosteric site of human liver pyruvate kinase upon activator binding include the breakage of an intersubunit cation-π bond, Acta Crystallogr F Struct Biol Commun 75 (Pt 6) (2019) 461–469. doi:10.1107/S2053230X19007209.

[42] T. Holyoak, B. Zhang, J. Deng, Q. Tang, C. B. Prasannan, A. W. Fenton, Energetic coupling between an oxidizable cysteine and the phosphorylatable N-terminus of human liver pyruvate kinase, Biochemistry 52 (3) (2013) 466–76. doi:10.1021/bi301341r.

[43] M. Chan, T.-S. Sim, Functional analysis, overexpression, and kinetic characterization of pyruvate kinase from *Plasmodium falciparum*, Biochem Biophys Res Commun 326 (1) (2005) 188–96. doi:10.1016/j.bbrc.2004.11.018.

[44] V. L. Knowles, C. S. Smith, C. R. Smith, W. C. Plaxton, Structural and regulatory properties of pyruvate kinase from the *Cyanobacterium synechococcus* PCC 6301, J Biol Chem 276 (24) (2001) 20966–72. doi:10.1074/jbc.M008878200.

[45] E. L. Auslender, S. Dorion, S. Dumont, J. Rivoal, Expression, purification and characterization of *Solanum tuberosum* recombinant cytosolic pyruvate kinase, Protein Expr Purif 110 (2015) 7–13. doi:10.1016/j.pep.2014.12.015.

[46] J. B. Peterson, H. J. Evans, Properties of pyruvate kinase from soybean nodule cytosol, Plant Physiol 61 (6) (1978) 909–14. doi:10.1104/pp.61.6.909.

[47] C. T. Evans, C. Ratledge, Partial purification and properties of pyruvate kinase and its regulatory role during lipid accumulation by the oleaginous yeast *Rhodosporidium toruloides* CBS 14, Canadian Journal of Microbiology 31 (5) (1985) 479–484. arXiv:https://doi.org/10.1139/m85-089, doi:10.1139/m85-089.
URL https://doi.org/10.1139/m85-089

[48] R. Etges, A. J. Mukkada, Purification and characterization of a metabolite-regulated pyruvate kinase from *Leishmania major* promastigotes, Mol Biochem Parasitol 27 (2-3) (1988) 281–9. doi:10.1016/0166-6851(88)90048-5.

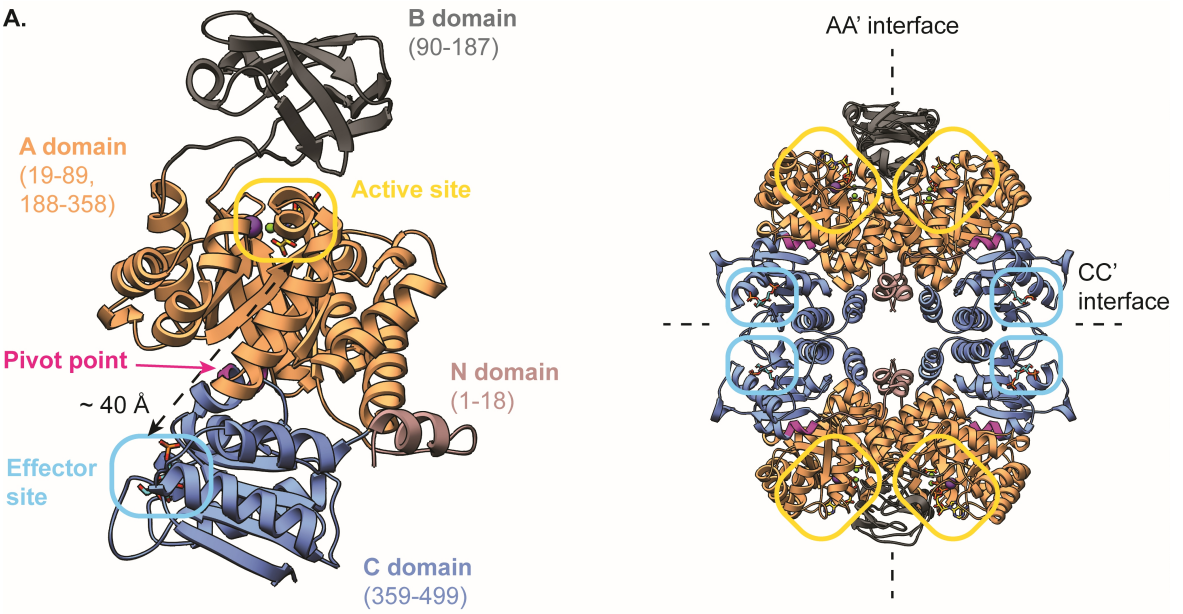

B.

```
1          11         21         31         41         51         61
MSQLQHNIGL SIFEPVAKHR ANRIICTIGP STQSVEALKG LMKSGMSVAR MNFSHGSYEY HQTTINNVRA
MSQLEHNIGL SIFEPVAKHR ANRIVCTIGP STQSVEALKN LMKSGMSVAR MNFSHGSHEY HQTTINNVRA

71         81         91         101        111        121        131
AAAELGLHIG IALDTKGPEI RTGLFKDGEA TYAPGDTVLV TTDPAFEKIG TKEKFYVDYP QLPNVVRPGG
AAAELGLHIG IALDTKGPEI RTGLFKDGEV SFAPGDIVCV TTDPAYEKVG TKEKFYIDYP QLTNAVRPGG

141        151        161        171        181        191        201
LIYVDDGVLT LRVLSKEDDC TLKCHVNNHH RLTDRKGINL PGCEVDLPAV SEKDRKDLQF GVEQGVDMIF
SIYVDDGVMT LRVVSKEDDR TLKCHVNNHH RLTDRRGINL PGCEVDLPAV SEKDRKDLEF GVAQGVDMIF

211        221        231        241        251        261        271
ASFIRTADQV REVRAALGEK GKDTLIISKI ENHQGVQNID AIIEASDGIM VARGDLGVEI PAEKVVVAQM
ASFIRTAEQV REVRAALGEK GKDILIISKI ENHQGVQNID SIIEASNGIM VARGDLGVEI PAEKVCVAQM

281        291        301        311        321        331        341
CIISKCNVAG KPVICATQML ESMTTNPRPT RAEVTDVANA VFNGADCVML SGETAKGKYP NEVVQYMVRI
CIISKCNVVG KPVICATQML ESMTSNPRPT RAEVSDVANA VLNGADCVML SGETAKGKYP NEVVQYMARI

351        361        371        381        391        401        411
CIEAQSATHD SVMFNSIKNL QKIPMSPEEA VCSSAVSSAF EVQAKAILVL SNTGRSARLI SKYRPNCPII
CVEAQSATHD TVMFNSIKNL QKIPMCPEEA VCSSAVASAF EVQAKAMLVL SNTGRSARLI SKYRPNCPII

421        431        441        451        461        471        481
CATTRLLTCR QLNVTRSVES VYYDVDAHGE DNDREKRVQL GVDWAKTKGY VSAGDVMVIV HADHSVKGYP
CVTTRLQTCR QLNVTRSVVS VFYDAAKSGE DKDKEKRVKL GLDFAKKEKY ASTGDVVVVV HADHSVKGYP

491
NQTRLVRVR  T. congolense PYK (G0UYF4)
NQTRLIYLP  T. b. brucei PYK (P30615)
```

- AA' interface
- active site
- effector site
- CC' interface

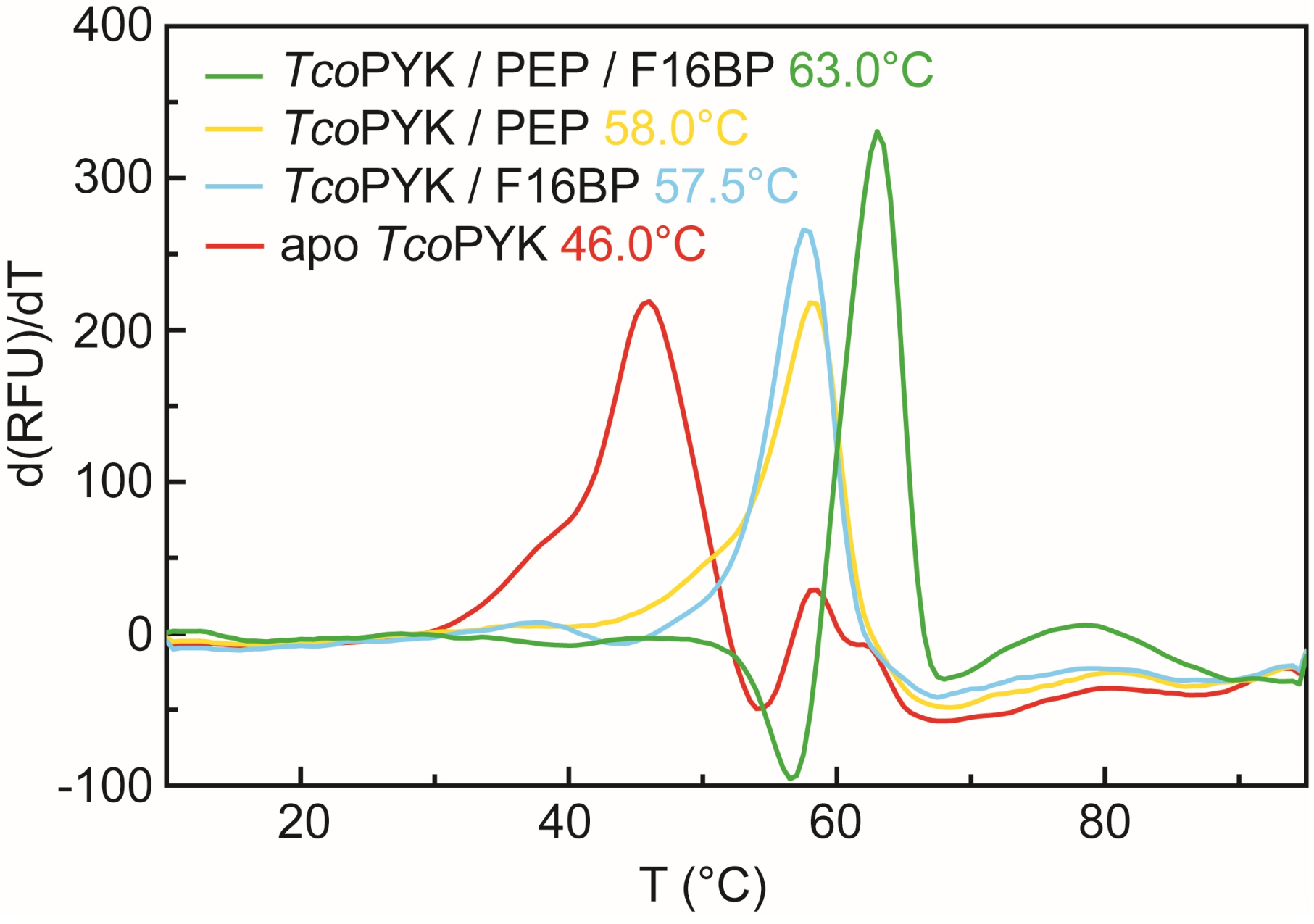
400
300
200
100
0
-100
d(RFU)/dT
20
40
60
80
T (°C)
TcoPYK / PEP / F16BP 63.0°C
TcoPYK / PEP 58.0°C
TcoPYK / F16BP 57.5°C
apo TcoPYK 46.0°C

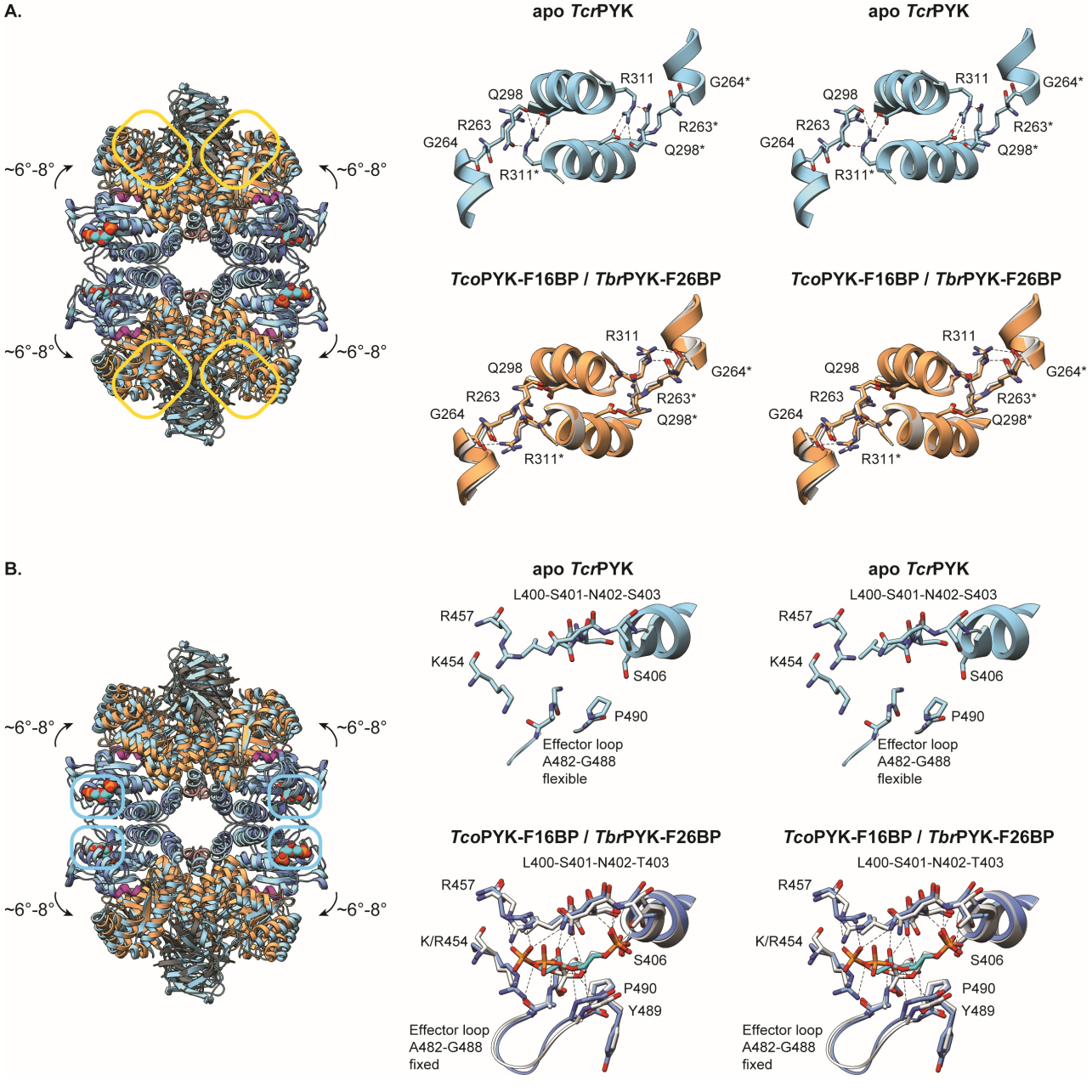
A.
~6°-8°
~6°-8°
~6°-8°
~6°-8°
apo TcrPYK
R311
G264*
Q298
R263
R263*
G264
Q298*
R311*
apo TcrPYK
R311
G264*
Q298
R263
R263*
G264
Q298*
R311*
TcoPYK-F16BP / TbrPYK-F26BP
R311
Q298
G264*
R263
R263*
G264
Q298*
R311*
TcoPYK-F16BP / TbrPYK-F26BP
R311
Q298
G264*
R263
R263*
G264
Q298*
R311*
B.
~6°-8°
~6°-8°
~6°-8°
~6°-8°
apo TcrPYK
L400-S401-N402-S403
R457
K454
S406
P490
Effector loop
A482-G488
flexible
apo TcrPYK
L400-S401-N402-S403
R457
K454
S406
P490
Effector loop
A482-G488
flexible
TcoPYK-F16BP / TbrPYK-F26BP
L400-S401-N402-T403
R457
K/R454
S406
P490
Y489
Effector loop
A482-G488
fixed
TcoPYK-F16BP / TbrPYK-F26BP
L400-S401-N402-T403
R457
K/R454
S406
P490
Y489
Effector loop
A482-G488
fixed

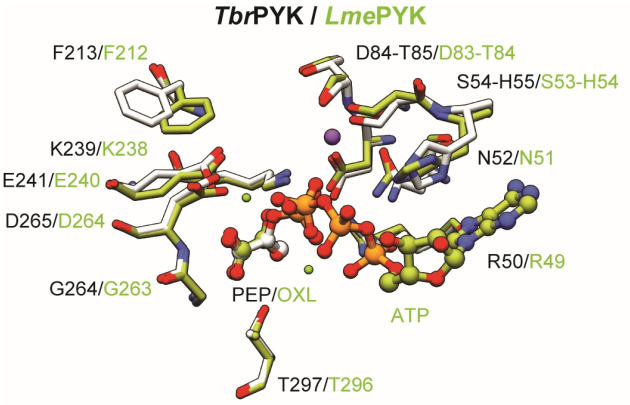
*Tbr*PYK / *Lme*PYK
F213/F212
D84-T85/D83-T84
S54-H55/S53-H54
K239/K238
N52/N51
E241/E240
D265/D264
R50/R49
G264/G263
PEP/OXL
ATP
T297/T296

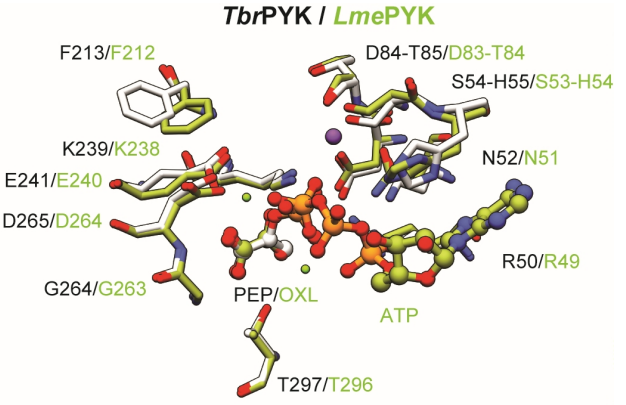
*Tbr*PYK / *Lme*PYK
F213/F212
D84-T85/D83-T84
S54-H55/S53-H54
K239/K238
N52/N51
E241/E240
D265/D264
R50/R49
G264/G263
PEP/OXL
ATP
T297/T296

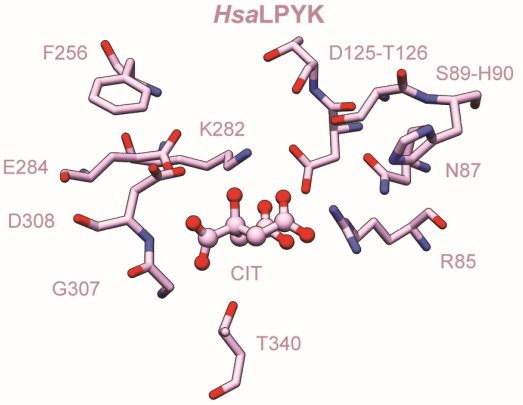
*Hsa*LPYK
F256
D125-T126
S89-H90
K282
E284
N87
D308
R85
CIT
G307
T340

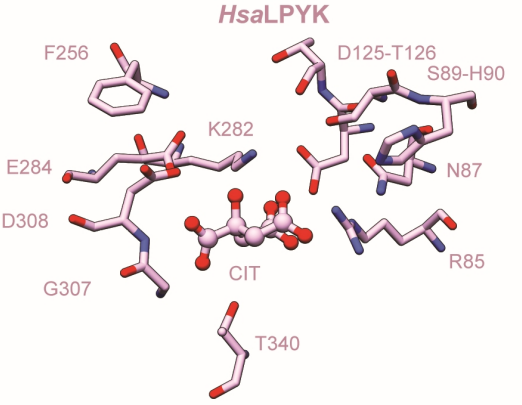
*Hsa*LPYK
F256
D125-T126
S89-H90
K282
E284
N87
D308
R85
CIT
G307
T340

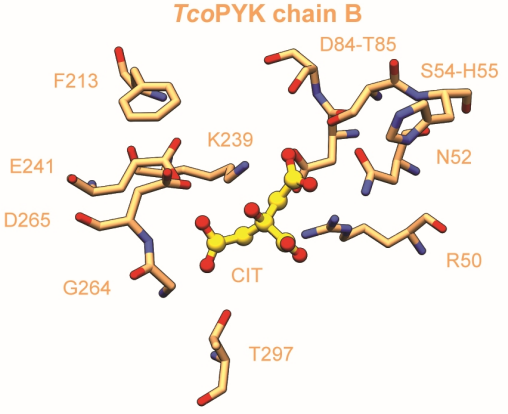
*Tco*PYK chain B
D84-T85
F213
S54-H55
K239
E241
N52
D265
R50
CIT
G264
T297

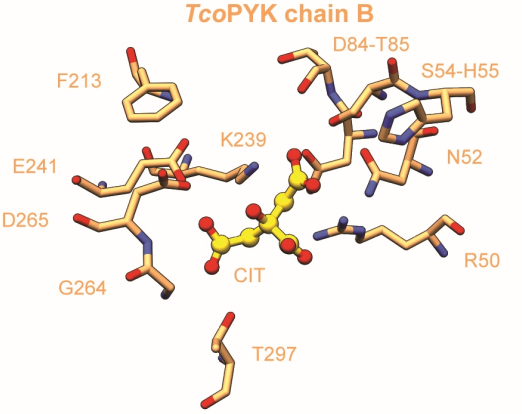
*Tco*PYK chain B
D84-T85
F213
S54-H55
K239
E241
N52
D265
R50
CIT
G264
T297

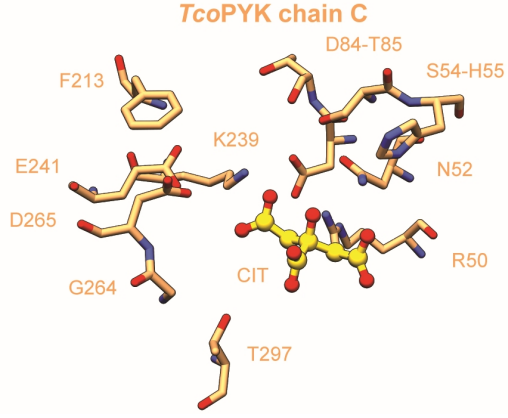
*Tco*PYK chain C
D84-T85
F213
S54-H55
K239
E241
N52
D265
R50
CIT
G264
T297

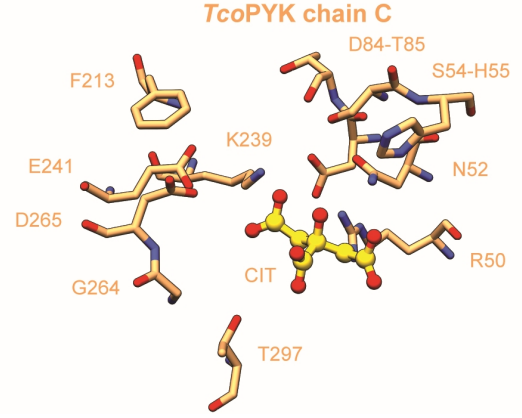
*Tco*PYK chain C
D84-T85
F213
S54-H55
K239
E241
N52
D265
R50
CIT
G264
T297

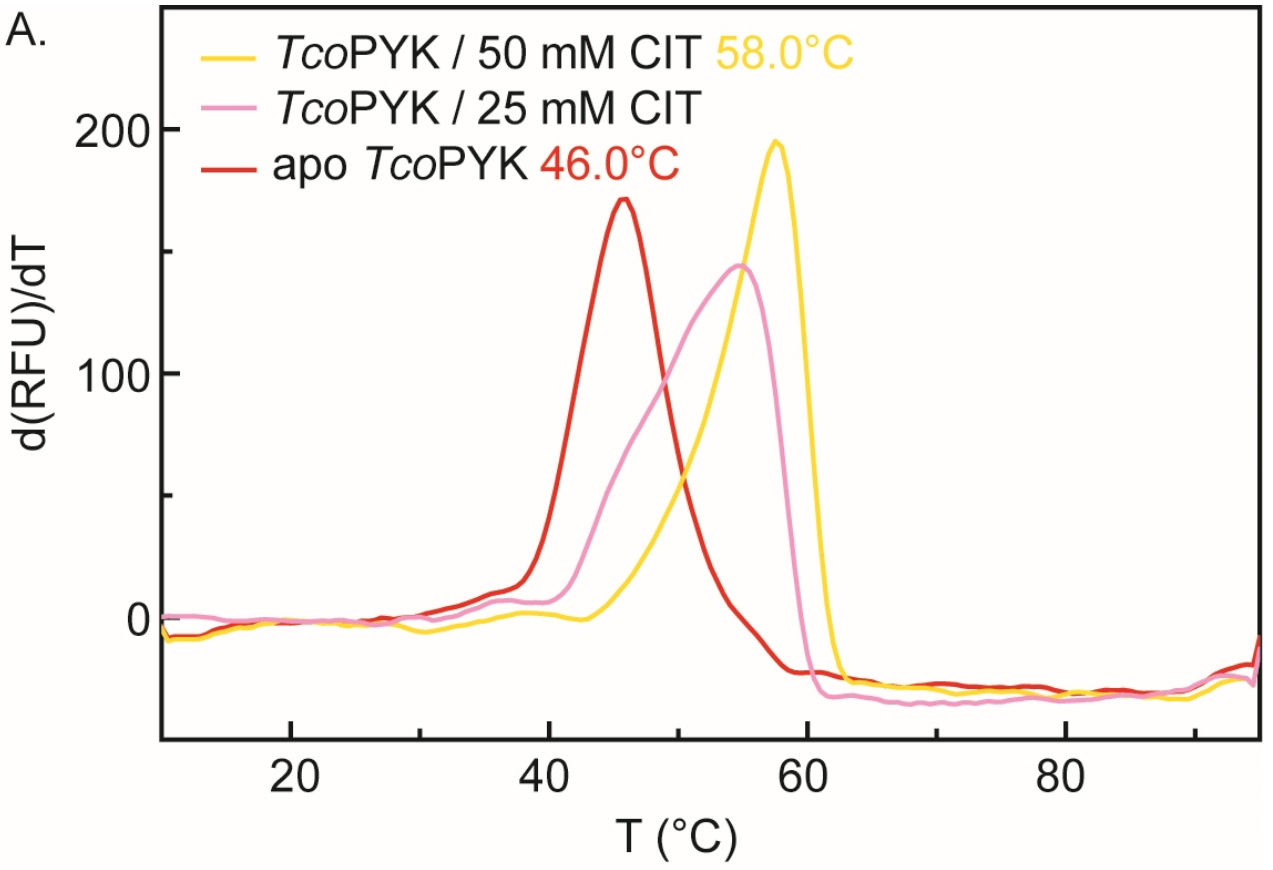
A.
TcoPYK / 50 mM CIT 58.0°C
TcoPYK / 25 mM CIT
apo TcoPYK 46.0°C
d(RFU)/dT
200
100
0
20
40
60
80
T (°C)

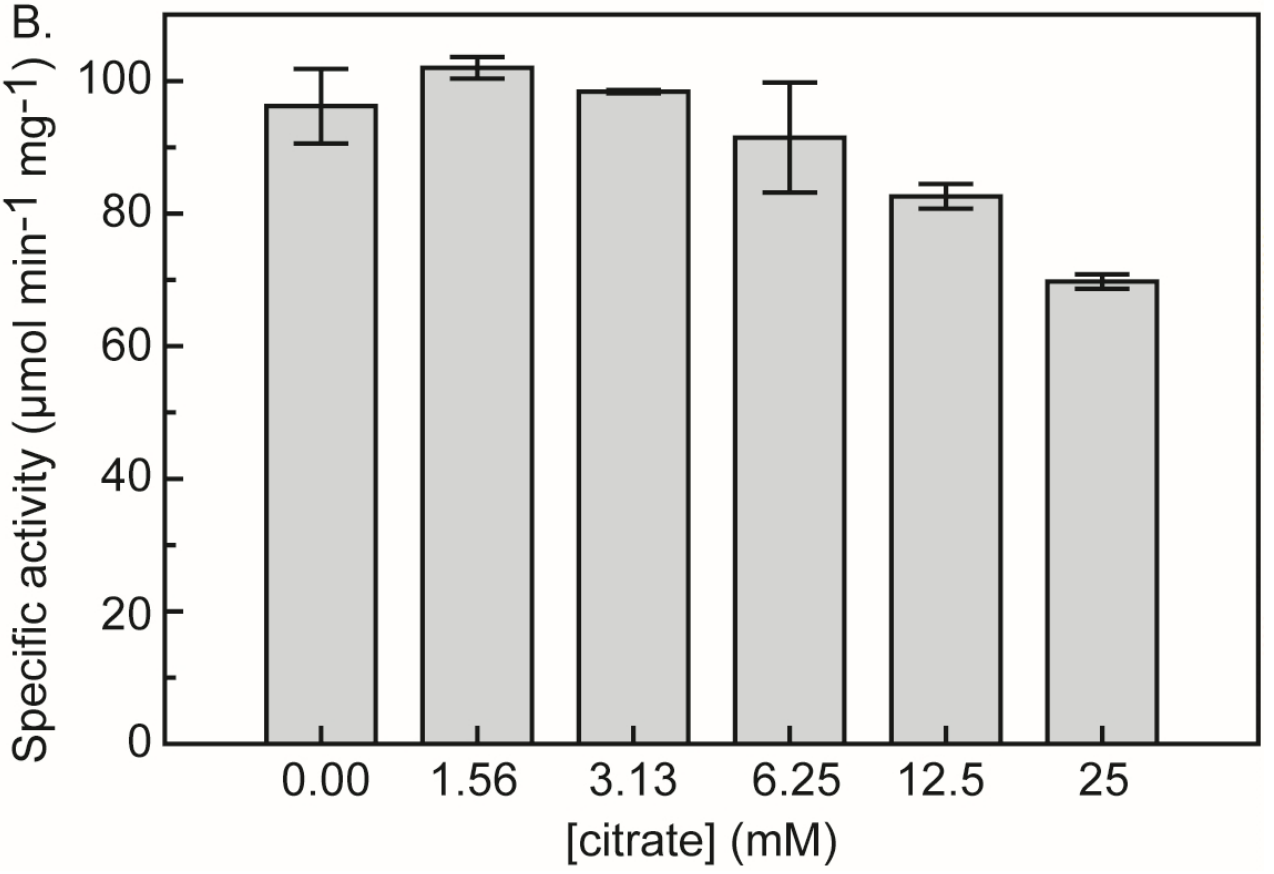
B.
Specific activity (µmol min-1 mg-1)
100
80
60
40
20
0
0.00
1.56
3.13
6.25
12.5
25
[citrate] (mM)

Author statement

Joar Esteban Pinto Torres: Conceptualization, Methodology, Validation, Formal analysis, Investigation, Resources, Data Curation, Writing - Original Draft, Writing - Review & Editing, Visualization, Supervision, Project administration. **Meng Yuan**: Conceptualization, Methodology, Validation, Formal analysis, Investigation, Resources, Data Curation, Writing - Original Draft, Writing - Review & Editing, Supervision. **Julie Goossens**: Investigation, Writing - Original Draft, Writing - Review & Editing. **Wim Versées**: Conceptualization, Formal analysis, Writing - Original Draft, Writing - Review & Editing. **Guy Caljon**: Writing - Original Draft, Writing - Review & Editing. **Paul A. Michels**: Conceptualization, Formal analysis, Writing - Original Draft, Writing - Review. **Malcolm D. Walkinshaw**: Conceptualization, Formal analysis, Writing - Original Draft, Writing - Review. **Stefan Magez**: Conceptualization, Methodology, Validation, Formal analysis, Investigation, Resources, Data Curation, Writing - Original Draft, Writing - Review & Editing, Visualization, Supervision, Project administration, Funding acquisition. **Yann G.-J. Sterckx**: Conceptualization, Methodology, Validation, Formal analysis, Investigation, Resources, Data Curation, Writing - Original Draft, Writing - Review & Editing, Visualization, Supervision, Project administration, Funding acquisition.